RF Switched-Capacitor Power Amplifier Modeling

Paul P. Sotiriadis, *Senior Member, IEEE*, Christos G. Adamopoulos, *Member, IEEE*, Dimitrios Baxevanakis, *Graduate Student Member, IEEE*, Panagiotis G. Zarkos, *Student Member, IEEE*, and Iason Vassiliou, *Member, IEEE*

***Abstract*—Detailed state-space modeling and analysis of a class of RF switched-capacitor power amplifiers achieving high efficiency, output power, and linearity are presented. Time-domain voltage and current waveforms are analytically obtained via the steady-state solution of the amplifier's model equations. The output power of the fundamental and that of the harmonics, as well as the drain efficiency of the switched-capacitor power amplifier (SCPA) are derived. The state-space model is implemented in MATLAB and all theoretical results are compared to Cadence Spectre simulation of the SCPA and are found to be in good agreement.**

***Index Terms*—Drain efficiency (DE), harmonic distortion, power amplifier (PA), state-space, steady-state, switched-capacitor.**

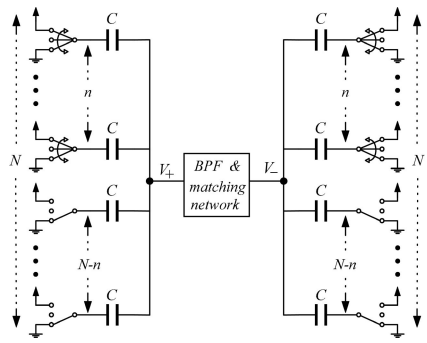

Fig. 1. Basic configuration of the differential SCPA.

I. Introduction

DIGITALLY modulated power amplifiers (DPAs) consisting of unit power amplifier (PA) cells have been an active area of research, effectively addressing many of the issues regarding the tradeoff between linearity and efficiency [1]–[4]. Based on the digital amplitude codeword, certain unit cells are selected to be switched at the carrier frequency. Change of the codeword implies a change of the set of switching unit cells, and a change of the output amplitude. For each unit cell, a switching PA is used achieving high efficiency.

The switched-capacitor PA (SCPA) considered in this work is a case of a DPA offering numerous advantages [5], [6]. To the best of our knowledge, it was first presented in [7] and it has been employed in various PA designs since then [8]–[12]. The core of the SCPA is formed of an array of N capacitors, a number of which (depending on the codeword applied at the input [7]) are being switched between V_{dd} and ground at the RF carrier frequency; the rest of them are connected to ground. In the simplest case, all capacitors are of the same size and the corresponding scheme is shown in Fig. 1, in differential form. Here, we assume that the first n capacitors are selected to switch and the last $N - n$ are held grounded.

This work extends [13] and provides a complete, detailed, and rigorous mathematical differential SCPA model. Using this model, an efficient MATLAB simulation engine is developed for quick initial evaluation of the amplifier's design parameters. The analytical steps of the presented framework could allow the adaptation of the proposed model to other classes of switching PAs, based on the same methodology principles and steps.

The remainder of this article is organized as follows. In Section II, the state-space modeling and analysis of the SCPA is presented. Section III derives the output and supply power using the results of Section II. Simulation results from both MATLAB and Cadence Spectre are presented in Section IV, validating the accuracy of the proposed model. Finally, Section V concludes this article.

II. State-Space Modeling of the SCPA

We use state-space modeling to derive the time-domain behavior of the SCPA proposed in [7]. It is preferred to harmonic balance and its derivatives because of the sharp switching, strong nonlinearity, and the tri-stated operation of the nMOS–pMOS pairs (inverters) in the SCPA.

A. SCPA's Time-Dependent Linear Model

The unit cell of the SCPA is shown in Fig. 2, with the circuit model elements that we take into account drawn in dashed-line. The switches of the unit cell are composed of nMOS–pMOS pairs, operating in a closed-open fashion [7]. When closed, they are modeled by equivalent conductances g_n

Manuscript received February 19, 2020; revised July 12, 2020; accepted August 24, 2020. Date of publication September 18, 2020; date of current version July 19, 2021. This work was supported in part by the Broadcom Foundation USA, and is co-financed by Greece and the European Union (European Social Fund-ESF) through the Operational Programme "Human Resources Development, Education and Lifelong Learning" in the Context of the Project "Strengthening Human Resources Research Potential via Doctorate Research" under Grant MIS-5000432, implemented by the State Scholarships Foundation (IKY). This article was recommended by Associate Editor P. Li. *(Corresponding author: Paul P. Sotiriadis.)*

Paul P. Sotiriadis and Dimitrios Baxevanakis are with the Department of Electrical and Computer Engineering, National Technical University of Athens, 157 80 Athens, Greece (e-mail: pps@ieee.org).

Christos G. Adamopoulos and Panagiotis G. Zarkos are with the Department of EECS, Berkeley Engineering, Berkeley, CA 94720 USA.

Iason Vassiliou is with Broadcom Hellas, 174 55 Athens, Greece.

Digital Object Identifier 10.1109/TCAD.2020.3025207

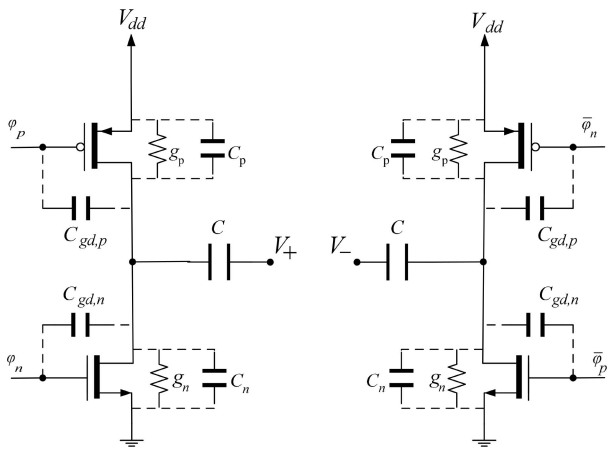

Fig. 2. Complementary unit cell of the differential SCPA.

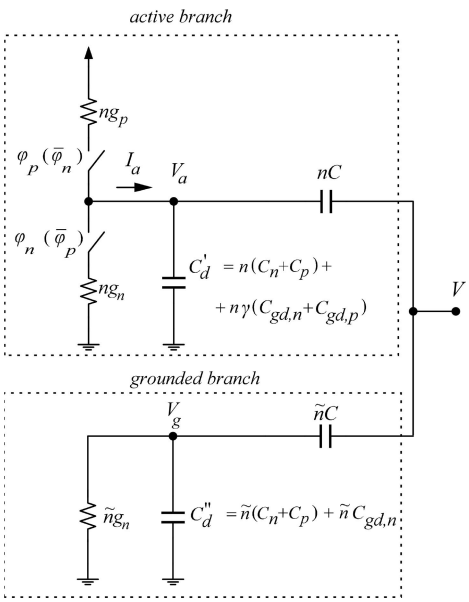

Fig. 3. Switches' network of the SCPA.

and g_p, respectively, in parallel with capacitors C_n and C_p capturing the parasitic capacitances at the drains of the transistors and the bottom-plate of C (assuming it is toward the switching pair). When open, conductances g_n and g_p are considered zero. To obtain a more accurate model, the C_{gd} capacitances are also included.

The SCPA in Fig. 1 is formed of N identical unit cells. We assume that the first n ($n = 0, 1, \ldots, N$) of them are active and operate in parallel, switching their outputs simultaneously between V_{dd} and ground at the RF carrier frequency. The remaining $\tilde{n} = N - n$ ones have grounded outputs with the pMOS being continuously off and the nMOS being in triode.

Fig. 3 shows the single-side linear model of the whole set of the N unit cells (when $0 < n < N$). The n active cells are combined parallel. Similarly for the $\tilde{n} = N - n$ grounded ones. Note that connecting C_p to ground, instead of V_{dd}, does not effect the time-behavior of the circuit, neither the period-average power consumption from V_{dd}.

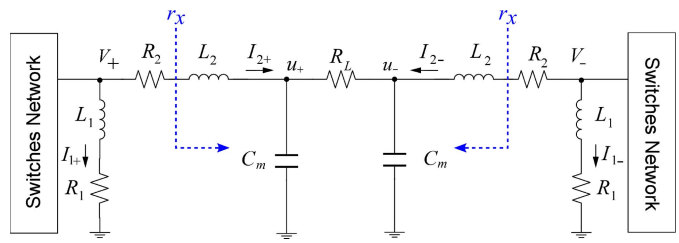

Fig. 4. Matching network and differential load.

The two modes of operation, active and grounded, imply the two different linear models as shown in the two branches of Fig. 3.

In the active cell branch (top), the nMOS and pMOS switch periodically between the off and the triode states implying time variation of the parasitic capacitances, especially of C_{gd}. To derive an analytical solution we need to use some average values of them. Assuming that the transistors are in triode about half the RF cycle one can choose the time-average value $\overline{C}_{gd}^{\text{active}} \simeq C_{gd}^{\text{triode}}/2$, where $C_{gd}^{\text{triode}} \simeq WLC_{ox}/2$. We also need to take into account the Miller effect due to the inversely switching input of the unit cells, implying a multiplication factor 2 for the C_{gd}. Capacitor C_{gd} however flips value between C_{gd}^{triode} and the negligible $C_{gd}^{\text{sat}} = WL_{ov}C_{ox}$. Therefore, the effective total paracitic capacitance due to C_{gd} of the nMOS and pMOS is $\gamma(C_{gd,n} + C_{gd,p})$ where $C_{gd,n/p} = C_{gd,n/p}^{\text{triode}}$ and $1/2 < \gamma < 1$, as shown in Fig. 3.

In the grounded cell branch (bottom of Fig. 3), the pMOS is continuously off and so its C_{gd} is practically zero, while the nMOS is always in triode and so $\overline{C}_{gd}^{\text{grounded}} = C_{gd}^{\text{triode}}$.

The total drain capacitances of the active and grounded cell branches are denoted by C_d' and C_d'', respectively, as shown in Fig. 3.

The switches' network of the N unit cells is followed by the tuning and matching network shown in Fig. 4. L_1 is used to tune the total capacitance $NC = (n + \tilde{n})C$ at the carrier frequency, while L_2 and capacitor C_m comprise the low-pass matching network employed for the impedance transformation and the suppression of harmonics. R_1 and R_2 model the finite Q of inductors L_1 and L_2, respectively. Power supply bondwire inductance is assumed to be much smaller than L_1, L_2, and thus to have a negligible effect at the RF carrier frequency; so, it is ignored in the analysis. The load, R_L, is transformed to the termination resistance r_x (single-sided) by L_2 and C_m.

B. Timing of the SCPA's Operation

The nMOS and pMOS switches of the unit cells are driven by non-overlapping clocks ϕ_n and ϕ_p, as shown in Fig. 5, [7], to eliminate crowbar currents during switching transitions. These non-overlapping pulses result in a tri-stated operation of the switching cell of Fig. 3 with three possible phases: 1) *Up-Down*;[1] 2) *Down-Up*; and 3) *Open*. Parameter D is defined as

[1] *Up-Down* refers to the state of SCPA model of Fig. 4, where the output of the positive (left) switches' network is *Up* and that of the negative (right) switches' network is *Down*, i.e., $V_+ = V_{dd}$, $V_- = 0$. Respectively, for the *Down-Up* state.

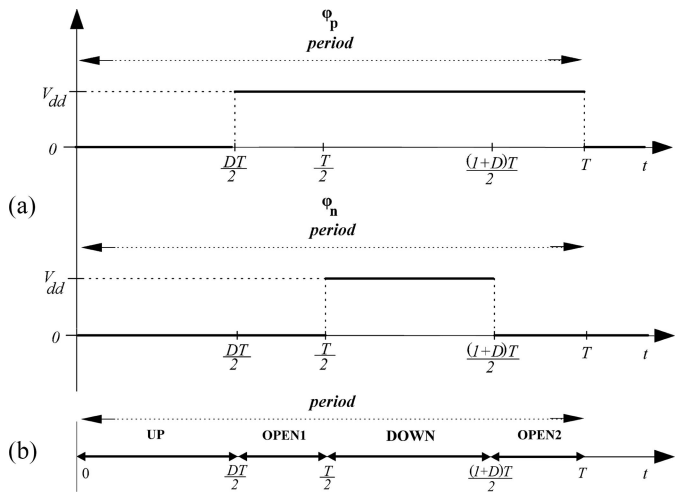

Fig. 5. Timing diagram and non-overlapping clocks. (a) Non-overlapping clock waveforms over one period. (b) Timing diagram of the positive (left) branch of the differential SCPA showing the four phases.

the ratio of the time-length during which the nMOS or pMOS switch is on, to the length of half a period, i.e., $T/2$.

The differential version of the circuit dictates appropriate timing of the two complementary branches, resulting in four timing phases within a period: 1) *Up-Down*; 2) *Open1*; 3) *Down-Up*; and 4) *Open2*. Complementary clocks $\overline{\phi_n}$ and $\overline{\phi_p}$ drive the nMOS and pMOS switches of the complementary branches, respectively. It is assumed that the transitions of the transistors from triode to off and vice-versa are instantaneous.

C. Equations Modeling the SCPA's Operation

Assuming[2] $0 < n < N$ for the circuits in Figs. 3 and 4 and setting $g_L = 1/R_L$

$$V_{a\pm} : I_{a\pm} = C'_d \dot{V}_{a\pm} + nC\big(\dot{V}_{a\pm} - \dot{V}_{\pm}\big) \tag{1}$$
$$V_{g\pm} : \tilde{n} g_n V_{g\pm} + C''_d \dot{V}_{g\pm} + \tilde{n} C\big(\dot{V}_{g\pm} - \dot{V}_{\pm}\big) = 0 \tag{2}$$
$$V_{\pm} : nC\big(\dot{V}_{a\pm} - \dot{V}_{\pm}\big) + \tilde{n} C\big(\dot{V}_{g\pm} - \dot{V}_{\pm}\big) = I_{1\pm} + I_{2\pm} \tag{3}$$
$$u_{\pm} : I_{2\pm} = C_m \dot{u}_{\pm} + g_L(u_{\pm} - u_{\mp}) \tag{4}$$
$$I_{1\pm} : V_{\pm} = L_1 \dot{I}_{1\pm} + R_1 I_{1\pm} \tag{5}$$
$$I_{2\pm} : V_{\pm} = R_2 I_{2\pm} + L_2 \dot{I}_{2\pm} + u_{\pm}. \tag{6}$$

Current $I_{a\pm}$ is expressed for each operating phase as

$$\begin{aligned} \text{Up Phase: } I_{a\pm} &= n g_p (V_{dd} - V_{a\pm}) \\ \text{Open Phase: } I_{a\pm} &= 0 \\ \text{Down Phase: } I_{a\pm} &= -n g_n V_{a\pm}. \end{aligned} \tag{7}$$

It is convenient to express (1)–(7) in matrix form. To this end we define the state vector $x \in \mathbb{R}^{12\times 1}$

$$x = \big[\, V_{a+},\, V_{g+},\, V_{+},\, u_{+},\, I_{1+},\, I_{2+},\, V_{a-},\, V_{g-},\, V_{-},\, u_{-},\, I_{1-},\, I_{2-} \big]^T \tag{8}$$

[2]If $n = 0$, the amplifier is not operating. If $n = N$, nodes $V_{g\pm}$ disappear from the model in Figure 3; eq. (2) should be removed, and all entries corresponding to $V_{g\pm}$ in the matrices should be removed accordingly.

as well as matrix $M = \begin{bmatrix} M_i & 0_{6\times 6} \\ 0_{6\times 6} & M_i \end{bmatrix} \in \mathbb{R}^{12\times 12}$ with $M_i \in \mathbb{R}^{6\times 6}$

$$M_i = \begin{bmatrix} C'_d + nC & 0 & -nC \\ 0 & C''_d + \tilde{n}C & -\tilde{n}C \\ nC & \tilde{n}C & -NC \end{bmatrix} \bigoplus \begin{bmatrix} C_m & 0 & 0 \\ 0 & L_1 & 0 \\ 0 & 0 & L_2 \end{bmatrix}$$

where $0_{n\times m}$ is the $n \times m$ zero matrix, and $\bigoplus$ denotes the direct sum of matrices [14]. Then, for the four phases, we have the following.

1) Up-Down Phase:

$$M\dot{x} = H_{ud} x + h_{ud} \tag{9}$$

where

$$\begin{aligned} H_{ud} &= \begin{bmatrix} H_u & G_L \\ G_L & H_d \end{bmatrix} \in \mathbb{R}^{12\times 12} \\ h_{ud} &= \begin{bmatrix} n g_p V_{dd} & 0_{1\times 11} \end{bmatrix}^T \in \mathbb{R}^{12\times 1} \\ H_u &= \begin{bmatrix} -n g_p & 0 \\ 0 & -\tilde{n} g_n \end{bmatrix} \bigoplus H_i \in \mathbb{R}^{6\times 6} \\ H_d &= \begin{bmatrix} -n g_n & 0 \\ 0 & -\tilde{n} g_n \end{bmatrix} \bigoplus H_i \in \mathbb{R}^{6\times 6} \\ H_i &= \begin{bmatrix} 0 & 0 & 1 & 1 \\ 0 & -g_L & 0 & 1 \\ 1 & 0 & -R_1 & 0 \\ 1 & -1 & 0 & -R_2 \end{bmatrix} \in \mathbb{R}^{4\times 4} \\ G_L &= g_L h^T h \in \mathbb{R}^{6\times 6} \\ h &= \begin{bmatrix} 0 & 0 & 0 & 1 & 0 & 0 \end{bmatrix} \in \mathbb{R}^{1\times 6}. \end{aligned}$$

2) Open (1 and 2) Phase:

$$M\dot{x} = H_{op} x \tag{10}$$

where

$$\begin{aligned} H_{op} &= \begin{bmatrix} H_o & G_L \\ G_L & H_o \end{bmatrix} \in \mathbb{R}^{12\times 12} \\ H_o &= \begin{bmatrix} 0 & 0 \\ 0 & -\tilde{n} g_n \end{bmatrix} \bigoplus H_i \in \mathbb{R}^{6\times 6}. \end{aligned}$$

3) Down-Up Phase:

$$M\dot{x} = H_{du} x + h_{du} \tag{11}$$

where

$$\begin{aligned} H_{du} &= \begin{bmatrix} H_d & G_L \\ G_L & H_u \end{bmatrix} \in \mathbb{R}^{12\times 12} \\ h_{du} &= \begin{bmatrix} 0_{1\times 6} & n g_p V_{dd} & 0_{1\times 5} \end{bmatrix}^T \in \mathbb{R}^{12\times 1}. \end{aligned}$$

It can be verified that M is invertible. We define the matrices and vectors of (12) and use them to express (9)–(11) as in Table I, where x_0, x_1, x_2, and x_3 are the initial conditions of the four phases *Up-Down*, *Open1*, *Down-Up*, and *Open2*, respectively, during a period T

$$\begin{aligned} A_{ud} &= M^{-1} H_{ud} \in \mathbb{R}^{12\times 12}, \quad b_{ud} = M^{-1} h_{ud} \in \mathbb{R}^{12\times 1} \\ A_{op} &= M^{-1} H_{op} \in \mathbb{R}^{12\times 12} \\ A_{du} &= M^{-1} H_{du} \in \mathbb{R}^{12\times 12}, \quad b_{du} = M^{-1} h_{du} \in \mathbb{R}^{12\times 1}. \end{aligned} \tag{12}$$

TABLE I
DIFFERENTIAL EQUATIONS AND INITIAL CONDITIONS FOR THE FOUR OPERATING PHASES DURING A PERIOD T

Phase	Time Period	Init. Cond.	Diff. Equation
$Up-Down$	$\left[0, \frac{DT}{2}\right)$	x_0	$\dot{x} = A_{ud}x + b_{ud}$
$Open1$	$\left[\frac{DT}{2}, \frac{T}{2}\right)$	x_1	$\dot{x} = A_{op}x$
$Down-Up$	$\left[\frac{T}{2}, \frac{(1+D)T}{2}\right)$	x_2	$\dot{x} = A_{du}x + b_{du}$
$Open2$	$\left[\frac{(1+D)T}{2}, T\right)$	x_3	$\dot{x} = A_{op}x$

D. Derivation of the State Vector x(t)

The derivation of $x(t)$ over a period in closed form dictates the solution of the differential equations of Table I. This requires the derivation of the initial conditions x_0, x_1, x_2, and x_3. Since $x(t)$ is T-periodic, it is $x(T) = x_0$.

During the *Up-Down* phase the solution of the differential equation is expressed using the exponential matrix as

$$x(t) = e^{A_{ud}t}x_0 + \left(e^{A_{ud}t} - I_{12}\right)A_{ud}^{-1}b_{ud}$$

where I_n is the $n \times n$ identity matrix. Also $A_{ud} = M^{-1}H_{ud}$ is invertible since matrices M and H_{ud} are both invertible.

The solutions for all phases are shown in Table II and are valid for their corresponding time intervals. Please note the time shifts by $t_1 = t - (DT/2)$, $t_2 = t - (T/2)$, and $t_3 = t - ((1+D)T/2)$.

Due to continuity, at the end of the *Up-Down* phase it is

$$x_1 = x\left(\frac{DT}{2}\right) = e^{A_{ud}\frac{DT}{2}}x_0 + \left(e^{A_{ud}\frac{DT}{2}} - I_{12}\right)A_{ud}^{-1}b_{ud} \quad (13)$$

and at the end of the *Open1* phase

$$x_2 = x\left(\frac{T}{2}\right) = e^{A_{op}\frac{(1-D)T}{2}}x_1. \quad (14)$$

Similarly, at the end of the *Down-Up* phase it is

$$x_3 = x\left(\frac{(1+D)T}{2}\right) = e^{A_{du}\frac{DT}{2}}x_2 + \left(e^{A_{du}\frac{DT}{2}} - I_{12}\right)A_{du}^{-1}b_{du} \quad (15)$$

and since $x(T) = x(0) = x_0$ at the end of the *Open2* phase

$$x_0 = x(T) = e^{A_{op}\frac{(1-D)T}{2}}x_3. \quad (16)$$

To derive $x(t)$ within the period $[0, T)$ we need to find the initial conditions x_0, x_1, x_2, and x_3 of the four phases. Defining $E_{ud}, E_{op}, E_{du} \in \mathbb{R}^{12\times 12}$, and $G_{ud}, G_{du} \in \mathbb{R}^{12\times 1}$ as

$$E_{ud} = e^{A_{ud}\frac{DT}{2}}, \quad G_{ud} = \left(e^{A_{ud}\frac{DT}{2}} - I_{12}\right)A_{ud}^{-1}b_{ud}$$
$$E_{op} = e^{A_{op}\frac{(1-D)T}{2}}$$
$$E_{du} = e^{A_{du}\frac{DT}{2}}, \quad G_{du} = \left(e^{A_{du}\frac{DT}{2}} - I_{12}\right)A_{du}^{-1}b_{du}$$

equations (13)–(16) are written in matrix form whose solution gives $x_0 = (I_{12} - E_{op}E_{du}E_{op}E_{ud})^{-1}E_G$, $x_1 = E_{ud}x_0 + G_{ud}$, $x_2 = E_{op}x_1$, $x_3 = E_{du}x_2 + G_{du}$, with $E_G = E_{op}E_{du}E_{op}G_{ud} + E_{op}G_{du}$.

TABLE II
EXPRESSIONS OF $x(t)$ FOR THE FOUR PHASES

Phase	Expression of $x(t)$
$Up-Down$	$x(t) = e^{A_{ud}t}x_0 + \left(e^{A_{ud}t} - I_{12}\right)A_{ud}^{-1}b_{ud}$
$Open1$	$x(t) = e^{A_{op}t_1}x_1$
$Down-Up$	$x(t) = e^{A_{du}t_2}x_2 + \left(e^{A_{du}t_2} - I_{12}\right)A_{du}^{-1}b_{du}$
$Open2$	$x(t) = e^{A_{op}t_3}x_3$

III. OUTPUT AND SUPPLY POWER CALCULATION

Here, we derive the expressions of the RF output and supply power using the state-space analysis of Section II. The power of the fundamental frequency of the differential output, $u_{\text{out}}(t) = u_+(t) - u_-(t)$, is derived from the equations of Table II, while the total power is calculated using the Gramians of the state-space model. The supply power is derived last. Note that the output can be expressed as $u_{\text{out}}(t) = e_{4,10}^T x(t)$ where $e_{4,10}^T = [0, 0, 0, 1, 0, 0, 0, 0, 0, -1, 0, 0] \in \mathbb{R}^{1\times 12}$.

A. Fundamental Frequency Output Power

The desirable output power is that of the fundamental harmonic component u_{out}^F of u_{out}. An analytical expression of it can be derived by defining the two scalar integrals

$$J_k^c = \frac{2}{T}\int_{t_{ik}}^{t_{fk}} e_{4,10}^T x_k(t)\cos(\omega_c t)dt$$
$$J_k^s = \frac{2}{T}\int_{t_{ik}}^{t_{fk}} e_{4,10}^T x_k(t)\sin(\omega_c t)dt \quad (17)$$

where $\omega_c = 2\pi/T$ and $x_k(t)$ is the previously derived state-vector function in phase $k =$ *Up-Down*, *Open1*, *Down-Up*, and *Open2*, available in Table II. Also, t_{ik} and t_{fk} are the initial and final times of phase k as given in Table I. Then, we can express the fundamental component of u_{out} as

$$u_{\text{out}}^F(t) = \left(\sum_k J_k^c\right)\cos(\omega_c t) + \left(\sum_k J_k^s\right)\sin(\omega_c t).$$

The analytical expressions of J_k^c and J_k^s, $k =$ *Up-Down*, *Open1*, *Down-Up*, and *Open2* can be easily calculated. The same is true for $u_{\text{out}}^F(t)$ and its amplitude.

B. Calculation of the Total Output Power

The power of the output harmonics can be derived by calculating the total output power and subtracting from it that of the fundamental. Since $u_{\text{out}}(t) = u_+(t) - u_-(t)$, $u_+(t) = e_4^T x(t)$, and $u_-(t) = e_{10}^T x(t)$, the total RMS output power can be expressed as

$$P_{\text{out}} = \frac{1}{TR_L}\int_0^T (u_+(t) - u_-(t))^2 dt$$
$$= \frac{1}{TR_L}\left(e_4^T We_4 - 2e_4^T We_{10} + e_{10}^T We_{10}\right) \quad (18)$$

where $e_4^T = [0, 0, 0, 1, 0, 0, 0, 0, 0, 0, 0, 0] \in \mathbb{R}^{1\times 12}$, $e_{10}^T = [0, 0, 0, 0, 0, 0, 0, 0, 0, 1, 0, 0] \in \mathbb{R}^{1\times 12}$, and $W = \int_0^T x(t)x^T(t)dt \in \mathbb{R}^{12\times 12}$ is the Gramian matrix of the

dynamical system [15]. It is $W = W_{ud} + W_{o1} + W_{du} + W_{o2}$, where the $\mathbb{R}^{12\times 12}$ Gramians are given by

$$W_{ud} = \int_0^{DT/2} x(t)x^T(t)dt, \quad W_{o1} = \int_{DT/2}^{T/2} x(t)x^T(t)dt$$
$$W_{du} = \int_{T/2}^{(1+D)T/2} x(t)x^T(t)dt, \quad W_{o2} = \int_{(1+D)T/2}^{T} x(t)x^T(t)dt.$$

Gramian $W_k = \int_{t_{ik}}^{t_{fk}} x(t)x^T(t)dt$, k = *Up-Down*, *Open1*, *Down-Up*, and *Open2* can be derived by the procedure described in [15] using the Lyapunov matrix equation

$$A_k W_k + W_k A_k^T = -Q_k \tag{19}$$

where $Q_k = b_k(\int_{t_{ik}}^{t_{fk}} x^T(t)dt) + (\int_{t_{ik}}^{t_{fk}} x(t)dt)b_k^T + x_{ik}x_{ik}^T - x_{fk}x_{fk}^T \in \mathbb{R}^{12\times 12}$. Equation (19) can be written in vectorized form using Kronecker's product [16] as

$$(I_{12} \otimes A_k + A_k \otimes I_{12})\mathrm{vec}(W_k) = -\mathrm{vec}(Q_k).$$

Thus, for each phase k it is

$$\mathrm{vec}(W_k) = -(I_{12} \otimes A_k + A_k \otimes I_{12})^{-1}\mathrm{vec}(Q_k) \in \mathbb{R}^{144\times 1}. \tag{20}$$

C. Supply Power Calculation

As seen from Fig. 3, only the *Up* phase of each branch of the differential topology contributes to the supply power consumption, P_s, so

$$P_s = \frac{1}{T}V_{dd}\left(\int_0^{DT/2} I_{a+}dt + \int_{T/2}^{(1+D)T/2} I_{a-}dt\right). \tag{21}$$

It is $I_{a\pm} = ng_p(V_{dd} - V_{a\pm})$ during the *Up* phase of each branch, with $V_{a+}(t) = e_1^T x(t)$, $V_{a-}(t) = e_7^T x(t)$, where $x(t)$ is given in Table II (*Up-Down* and *Down-Up* phase, respectively), and $e_1^T = [1, 0, 0, 0, 0, 0, 0, 0, 0, 0, 0, 0] \in \mathbb{R}^{1\times 12}$, $e_7^T = [0, 0, 0, 0, 0, 0, 1, 0, 0, 0, 0, 0] \in \mathbb{R}^{1\times 12}$. Thus, we get

$$\begin{aligned} P_s = {} & ng_p DV_{dd}^2 - ng_p\frac{V_{dd}}{T} \\ & \times \left\{ e_1^T A_{ud}^{-1}\left[\left(e^{A_{ud}\frac{DT}{2}} - I_{12}\right)\left(x_0 + A_{ud}^{-1}b_{ud}\right) - \frac{DT}{2}b_{ud}\right] \right. \\ & \left. + e_7^T A_{du}^{-1}\left[\left(e^{A_{du}\frac{DT}{2}} - I_{12}\right)\left(x_2 + A_{du}^{-1}b_{du}\right) - \frac{DT}{2}b_{du}\right]\right\}. \end{aligned} \tag{22}$$

IV. Simulation Results

This section presents Cadence Spectre and MATLAB simulation results in 65 nm technology, verifying our theoretical development. Motivated by the work in [7], the carrier frequency f_c is 2.2 GHz and the unit cell capacitor C is 500 fF. Parameter D was set to 80%, while resistance r_x is selected to be 16 Ω. The on resistance, r_{on}, is chosen to be approximately 8 Ω. For the nMOS and pMOS transistors it is chosen $L_n = L_p = 90$ nm, $W_n = 48$ μm, and $W_p = 192$ μm to correspond to $r_{\mathrm{on}} = 8\,\Omega$. Finally, L_1 is chosen 0.16 nH to resonate with the total capacitance NC of the array, $C_m = 2.9$ pF and $L_2 = 1.45$ nH, while the load resistance is $R_L = 50\,\Omega$.

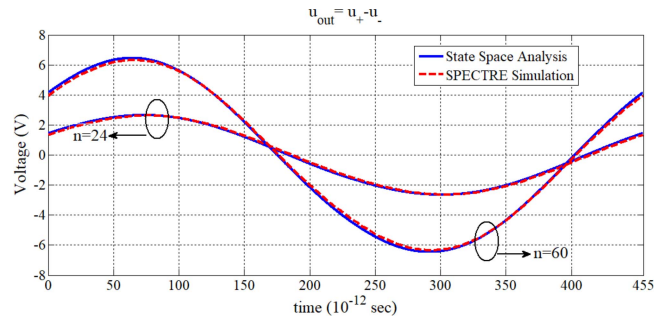

Fig. 6. Steady-state waveforms of u_{out}.

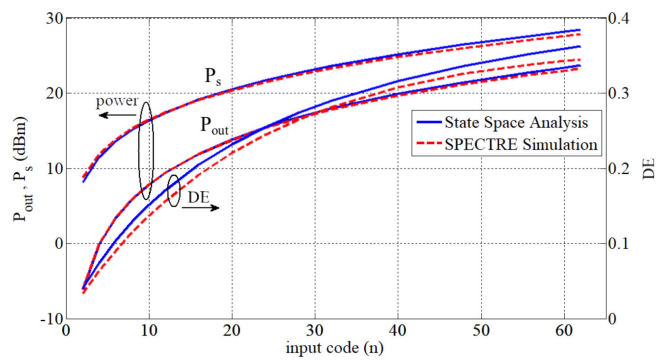

Fig. 7. Simulation and model results of P_{out}, P_s, and DE.

1) Time-Domain Waveforms: Fig. 6 presents the differential output voltage of the SCPA, as derived by the proposed model and by PSS simulation. The matching of the waveforms is reasonable; they differ in the transitions of the switches and some have a minor phase offset but these do not impact the estimation of the output power as it is illustrated in the following section. For the case of $n = 24$, the maximum instantaneous error normalized to the maximum amplitude value obtained by Cadence Spectre is less than 3.2%, while for the case of $n = 60$ it is less than 4.5%.

2) Output and Supply Power: The output power of the amplifier is presented in Fig. 7 as a function of the input code n. It can be seen that the estimated supply power is in good agreement with the simulation result; the maximum error of P_{out} is less than 0.44 dBm, and the maximum error of P_s is less than 0.61 dBm. The drain efficiency (DE) is also shown in Fig. 7. The analytically obtained efficiency is also a good approximation of the one derived via simulation, with the maximum error being less than 1.7%.

V. Conclusion

This article presents a detailed state-space modeling and analysis of a class of RF SCPAs with high efficiency, output power, and linearity. Time-domain voltage and current waveforms have been analytically obtained via the steady-state solution of the equations describing the amplifier's model. The analysis resulted in the derivation of the output and supply power of the SCPA as well as its DE and output harmonics power. MATLAB results have been verified with Cadence Spectre simulation of the SCPA in a 65 nm technology.

REFERENCES

[1] A. Kavousian, D. K. Su, M. Hekmat, A. Shirvani, and B. A. Wooley, "A digitally modulated polar cmos power amplifier with a 20-mhz channel bandwidth," *IEEE J. Solid-State Circuits*, vol. 43, no. 10, pp. 2251–2258, Oct. 2008.

[2] P. Cruise *et al.*, "A digital-to-RF-amplitude converter for GSM/GPRS/EDGE in 90-nm digital CMOS," in *IEEE Radio Freq. Integr. Circuits (RFIC) Symp. Dig. Papers*, Jun. 2005, pp. 21–24.

[3] C. D. Presti, F. Carrara, A. Scuderi, P. M. Asbeck, and G. Palmisano, "A 25 dbm digitally modulated cmos power amplifier for WCDMA/EDGE/OFDM with adaptive digital predistortion and efficient power control," *IEEE J. Solid-State Circuits*, vol. 44, no. 7, pp. 1883–1896, Jul. 2009.

[4] D. Chowdhury, L. Ye, E. Alon, and A. M. Niknejad, "An efficient mixed-signal 2.4-GHz polar power amplifier in 65-nm CMOS technology," *IEEE J. Solid-State Circuits*, vol. 46, no. 8, pp. 1796–1809, Aug. 2011.

[5] J. S. Walling, S.-M. Yoo, and D. J. Allstot, "Digital power amplifier: A new way to exploit the switched-capacitor circuit," *IEEE Commun. Mag.*, vol. 50, no. 4, pp. 145–151, Apr. 2012.

[6] J. S. Walling, "The switched-capacitor power amplifier: A key enabler for future communications systems," in *Proc. IEEE 45th Eur. Solid State Circuits Conf. (ESSCIRC)*, Sep. 2019, pp. 18–24.

[7] S.-M. Yoo, J. S. Walling, E. C. Woo, B. Jann, and D. J. Allstot, "A switched-capacitor RF power amplifier," *IEEE J. Solid-State Circuits*, vol. 46, no. 12, pp. 2977–2987, Dec. 2011.

[8] S. Yoo *et al.*, "A class-G switched-capacitor RF power amplifier," *IEEE J. Solid-State Circuits*, vol. 48, no. 5, pp. 1212–1224, May 2013.

[9] W. Yuan, V. Aparin, J. Dunworth, L. Seward, and J. S. Walling, "A quadrature switched capacitor power amplifier," *IEEE J. Solid-State Circuits*, vol. 51, no. 5, pp. 1200–1209, May 2016.

[10] Z. Bai, D. Johnson, A. Azam, A. Saha, W. Yuan, and J. S. Walling, "A 12 bit split-array switched capacitor power amplifier in 130 nm CMOS," in *Proc. 29th IEEE Int. Syst. Chip Conf. (SOCC)*, Sep. 2016, pp. 24–28.

[11] W. Yuan and J. S. Walling, "A multiphase switched capacitor power amplifier," *IEEE J. Solid-State Circuits*, vol. 52, no. 5, pp. 1320–1330, May 2017.

[12] S.-W. Yoo, S.-C. Hung, and S.-M. Yoo, "A Watt-level quadrature class-G switched-capacitor power amplifier with linearization techniques," *IEEE J. Solid-State Circuits*, vol. 54, no. 5, pp. 1274–1287, May 2019.

[13] P. G. Zarkos, C. G. Adamopoulos, I. Vassiliou, and P. P. Sotiriadis, "A mathematical model for time-domain analysis and for parametric optimization of a class of switched capacitor RF power amplifiers," in *Proc. 21st IEEE Int. Conf. Electron. Circuits Syst. (ICECS)*, Dec. 2014, pp. 518–521.

[14] R. A. Horn and C. R. Johnson, *Matrix Analysis*, 2nd ed. Cambridge, U.K.: Cambridge Univ. Press, 2013.

[15] P. Reynaert, K. L. R. Mertens, and M. S. J. Steyaert, "A state-space behavioral model for CMOS class E power amplifiers," *IEEE Trans. Comput.-Aided Design Integr. Circuits Syst.*, vol. 22, no. 2, pp. 132–138, Feb. 2003.

[16] P. Lancaster and M. Tismenetsky, *The Theory of Matrices With Applications* (Computer Science and Scientific Computing), 2nd ed. Cambridge, MA, USA: Acadamic, 1985.